AN ABSTRACT OF THE THESIS OF

Juan Manuel Vanegas for the degree of Master of Science in Biochemistry and Biophysics presented on September 18, 2007.
Title: Alkylation Kinetics of the Human Retinoid X Receptor α Using Cysteine as a Local Probe.

Abstract approved:

Michael I. Schimerlik

The unfolding of human retinoid X receptor α in the presence of the denaturant guanidine HCl was studied using stopped-flow absorbance spectroscopy. The protein's four native cysteine residues were mutated to obtain four single-cysteine mutants, each with the other three cysteine residues mutated to alanine. The thiols of these hRXRα mutants were alkylated with DTNB, Ellman's reagent, and the appearance of the product TNB was followed over time with a spectrophotometer at 412 nm. Alkylation of the amino acid L-cysteine by DTNB was also studied in order to provide a model system for the thiol-DTNB reaction. The kinetic analysis of the observed rates of reaction of the protein's cysteine residues with DTNB suggests that each thiol is in equilibrium between an open and a closed state, DTNB forms intermediates with both the open and closed forms of the thiol, but only the open-DTNB intermediate is alkylated. The energetic parameters obtained for the unfolding by GuHCl are well separated for each thiol, suggesting that the observed events represent local instead of global unfolding. Previous investigation of the global unfolding of hRXRα by Harder et al. (1) further supports the present hypothesis, as the midpoint of the observed unfolding events take place before the midpoint of global unfolding of the protein. Circular dichroism and tryptophan

fluorescence emission were used to determine structural differences between the mutants and the wild-type.

Alkylation Kinetics of the Human Retinoid X Receptor α Using Cysteine as a Local Probe

by
Juan Manuel Vanegas

A THESIS

submitted to

Oregon State University

in partial fulfillment of
the requirements for the
degree of

Master of Science

Presented September 18, 2007
Commencement June 2008

Master of Science thesis of Juan Manuel Vanegas presented on September 18, 2007.

APPROVED:

Major Professor, representing Biochemistry and Biophysics

Chair of the Department of Biochemistry and Biophysics

Dean of the Graduate School

I understand that my thesis will become part of the permanent collection of Oregon State University libraries. My signature below authorizes release of my thesis to any reader upon request.

Juan Manuel Vanegas, Author

ACKNOWLEDGMENTS

I would like to thank Dr. Michael Schimerlik for training a physicist to do biochemistry, and introducing me to the mysterious world of chemical kinetics. Great advice and devious biochemistry questions have helped me become a better scientist.

To Dr. David Broderick for his assistance in purifying the proteins, because without his help this would not have been possible. Although, I did not receive any instruction on wines and single malt scotch, as did Larry Rosenbaum, Dave's help was very important.

Last, but not least, I would like to thank my wife for her undivided support throughout this endeavor, and may I someday repay her for all the time I spend on this project and not with her.

CONTRIBUTION OF AUTHORS

Dr. Michael I. Schimerlik assisted with data analysis and interpretation, as well as contributing mathematical models. Dr. David Broderick assisted with protein purification. Site-directed mutagenesis of the pET 15b construct containing the hRXRα LBD (T226 to T462) was done by Rosalyn Upson.

TABLE OF CONTENTS

LIST OF FIGURES

LIST OF FIGURES (Continued)

Figure Page

LIST OF TABLES

LIST OF APPENDICES

LIST OF ABBREVIATIONS

GuHCl	Guanidine HCl; TCEP, Tris-2[carboxyethyl] phosphine
DTNB	5,5'-Dithio-bis(2-nitrobenzoic acid)
TNB	2-nitro-5-thiobenzoic acid
CHAPS	3-[(3-cholamidopropyl)-dimethylammonio]-1-propane sulfonate
hRXRα	human Retinoid X Receptor
LBD	Ligand Binding Domain
MutC269	hRXRα LBD (C369, C404, C432 →A) single-cysteine mutant
MutC369	hRXRα LBD (C269, C404, C432 →A) single-cysteine mutant
MutC404	hRXRα LBD (C269, C369, C432 →A) single-cysteine mutant
MutC432	hRXRα LBD (C269, C369, C404 →A) single-cysteine mutant
9cRA	9-cis-retinoic acid

Chapter 1

Introduction

Retinoic X and retinoic acid receptors form a family of ligand-activated transcriptional regulators, which control retinoic acids target genes through a diverse and complex signaling system (2). Retinoic acids are naturally occurring metabolites of vitamin A. RAR genes are activated by all-trans and 9-cis-retinoic acid, while RXR receptors are specific to 9-cis-retinoic acid. These nuclear receptors belong to a larger superfamily of transcription factors that share five to six conserved domains (2). Each one these regions performs a specific task, which may depend on the type of cell and the regulated gene. The first N-terminal region, known as A/B, contains a cell-specific transactivating function AF-1, followed by a DNA binding domain (region C) composed of two zinc fingers, a hinge section (region D), a ligand binding domain (region E), and sometimes a C-terminal domain of unknown function (2, 3). Both the A/B and E domains are cell and promoter specific, with the LBD showing strong dimerization (3).

1.1 - Physiology of RXR

RXR and RAR play an important role in cell development and differentiation. RXR is the heterodimeric partner, some of which require this dimerization for high-affinity DNA binding, of several nuclear receptors including RAR, thyroid hormone receptor, vitamin D receptor, perosixome proliferator-activated receptors, liver X receptors, farnesoid receptor, pregnane X receptor, and constitutive androstane receptor (3). RXR isoforms (α, β, and γ) are ubiquitously found in the body, with RXRα mainly distributed within the liver, lung, muscle, kidney, epidermis, and intestine, and is the

major isotype in the skin (4). RXR regulates target genes by binding to retinoic acids response elements (RAREs) (3), which are generally composed of direct repeats of the hexanucleotide sequence AGG/TTCA separated by 1, 2, or 5 bp (5). However, due to the promiscuous nature of RXR, its heterodimers can bind a variety of other response elements such as direct repeats, palindromes, and inverted palindromes (6, 7). This promiscuous nature of RXR also associates the receptor with a variety of diseases, extending from skin problems such as psoriasis and acne, to cancer and metabolic diseases such as diabetes and obesity (8). In the case of diabetes, rexinoids may reduce insulin resistance (3). Also, its role in cell proliferation and apoptosis makes RXR a potential target for cancer research.

1.2 - Structural Characterization of the RXR LBD

The LBD of RXRα forms homodimers and homotetramers in a concentration dependent manner, and addition of the ligand 9-cis-retinoic acid converts the tetramers into dimers regardless of concentration (9). Egea et al. (9) also showed that RXRα/RARα hetereodimers become more compact as 9cRA is bound, with the fully liganded dimer having the most compact structure. The crystal structure of the LBD homodimer of human RXRα (10) was the first reported structure for the RXR family, and it was also the first structure of a nuclear receptor LBD. Following the report of this structure, many other structures of RXR have been determined which include the RXRα LBD in tetrameric form (11), RXRγ LBD bound to all-trans retinoic acid (12), RXRα LBD homodimer bound to 9cRA (13), unliganded RXRα/RARα heterodimer (14), and a variety of homo and heterodimeric structures bound to other natural and synthetic agonists and antagonists, as well as co-activator peptides. RXRα LBD contains 12 alpha

helices and a small beta sheet region. The ligand binding site is buried in a hydrophobic environment located between the β sheet and helices 3, 5, 11, and 12. Binding of the ligand causes a conformational change in the protein described as a 'mousetrap' mechanism in which the final structure has helix 12 closing the binding pocket and trapping the ligand (3, 12).

Although the hRXRα LBD 3-dimensional structure has been previously characterized by crystal structures as mentioned earlier, little is known about the dynamics of the protein in solution. Hydrogen/Deuterium exchange of hRXRα LBD (15) results of 9cRA binding confirm the results observed in the crystal structures. However, residues in helices 7, 10 and 11, as well as in the H7-H8 and H10-H11 loops were unexpectedly shown to be protected, even though they are not directly in contact with the bound 9cRA. Additionally, global unfolding of RXR (1), as determined by circular dichroism and fluorescence emission, revealed that unfolding of the protein follows a minimal three state model with at least one monomeric intermediate.

1.3 - Objective of the Study

Human RXRα LBD contains four cysteine residues located along positions C269, C369, C404, and C432. None of these residues is involved in disulfide bonds as confirmed by the crystal structure. These four residues are spatially situated in different regions of the protein and under differing environments, which suggests that solvent accessibility as well as reactivity is expected to be unique for each cysteine. The reactivity of these residues can be measured by the rate of modification with the compound 5,5'-Dithio-bis(2-nitrobenzoic acid) (DTNB), as observed by the production of 2-nitro-5-thiobenzoic acid (TNB) which strongly absorbs light at 412 nm. Analysis of the

simultaneous modification of the four cysteines present in the hRXRα LBD may not allow discerning of the different rates of reaction if some of the phases are close in magnitude. Mutation of some of the cysteine residues can be used to independently study the rates of alkylation for each one. In the present study four mutants were created each containing only a single cysteine and the other cysteine residues were mutated to alanine as it is a good stearic analog. Because the mutation of these residues may affect the 3-dimensional structure of the protein, structural analyses of each hRXRα LBD mutant is important in assessing the validity of the results. Two methods were presently used to assess the structural changes: circular dichroism and fluorescence emission. Since RXR is mostly alpha – helical, circular dichroism reveals changes in overall alpha helical content. Parallel to the CD, the fluorescence emission provides information on changes in the environment of the two tryptophan residues present in the protein.

Chapter 2

Alkylation Kinetics of the Human Retinoid X Receptor α Using Cysteine as a Local Probe

Juan M. Vanegas[1], Michael I. Schimerlik[1], David Broderick[1],

Mark Leid[2], Max L. Deinzer[3]

[1]Department of Biochemistry and Biophysics, [2]Department of Pharmaceutical Science,

[3]Department of Chemistry, Oregon State University,

Corvallis, Oregon 97331

2.1 - Abstract

The unfolding of human retinoid X receptor α in the presence of the denaturant guanidine HCl was studied using stopped-flow absorbance spectroscopy. The protein's four native cysteine residues were mutated to obtain four single-cysteine mutants, each with the other three cysteine residues mutated to alanine. The thiols of these hRXRα mutants were alkylated with DTNB, Ellman's reagent, and the appearance of the product TNB was followed over time with a spectrophotometer at 412 nm. Alkylation of the amino acid L-cysteine by DTNB was also studied in order to provide a model system for the thiol-DTNB reaction. The kinetic analysis of the observed rates of reaction of the protein's cysteine residues with DTNB suggests that each thiol is in equilibrium between an open and a closed state, DTNB forms intermediates with both the open and closed forms of the thiol, but only the open-DTNB intermediate is alkylated. The energetic parameters obtained for the unfolding by GuHCl are well separated for each thiol, suggesting that the observed events represent local instead of global unfolding. Previous investigation of the global unfolding of hRXRα by Harder et al. (1) further supports the present hypothesis, as the midpoint of the observed unfolding events take place before the midpoint of global unfolding of the protein. Circular dichroism and tryptophan fluorescence emission were used to determine structural differences between the mutants and the wild-type.

Abbreviations: GuHCl, Guanidine HCl; TCEP, Tris-2[carboxyethyl] phospine; DTNB, 5,5'-Dithio-bis(2-nitrobenzoic acid); TNB, 2-nitro-5-thiobenzoic acid; CHAPS, 3-[(3-cholamidopropyl)-dimethylammonio]-1-propane sulfonate; hRXRα, human Retinoid X Receptor; LBD, Ligand Binding Domain; 9-cis-retinoic Acid, 9cRA;

MutC269, hRXRα LBD (C369, C404, C432 →A) single-cysteine mutant; MutC369, hRXRα LBD (C269, C404, C432 →A) single-cysteine mutant; MutC404, hRXRα LBD (C269, C369, C432 →A) single-cysteine mutant; MutC432, hRXRα LBD (C269, C369, C404 →A) single-cysteine mutant.

2.2 - Introduction

Retinoic X and retinoic acid receptors form a family of ligand-activated transcriptional regulators, which control retinoic acids target genes through a diverse and complex signaling system (2). Retinoic acids are naturally occurring metabolites of vitamin A. RAR genes are activated by all-trans and 9-cis-retinoic acid, while RXR receptors are specific to 9-cis-retinoic acid. These nuclear receptors belong to a larger superfamily of transcription factors that share five to six conserved domains (2). Each one these regions performs a specific task, which may depend on the type of cell and the regulated gene. The first N-terminal region, known as A/B, contains a cell-specific transactivating function AF-1, followed by a DNA binding domain (region C) composed of two zinc fingers, a hinge section (region D), a ligand binding domain (region E), and sometimes a C-terminal domain of unknown function (2, 3). Both the A/B and E domains are cell and promoter specific, with the LBD showing strong dimerization (3).

RXR and RAR play an important role in cell development and differentiation. RXR is the heterodimeric partner, some of which require this dimerization for high-affinity DNA binding, of several nuclear receptors including RAR, thyroid hormone receptor, vitamin D receptor, perosixome proliferator-activated receptors, liver X receptors, farnesoid receptor, pregnane X receptor, and constitutive androstane receptor (3). RXR isoforms (α, β, and γ) are ubiquitously found in the body, with RXRα mainly

distributed within the liver, lung, muscle, kidney, epidermis, and intestine, and is the major isotype in the skin (4). RXR regulates target genes by binding to retinoic acids response elements (RAREs) (3), which are generally composed of direct repeats of the hexanucleotide sequence AGG/TTCA separated by 1, 2, or 5 bp (5). However, due to the promiscuous nature of RXR, its heterodimers can bind a variety of other response elements such as direct repeats, palindromes, and inverted palindromes (6, 7). This promiscuous nature of RXR also associates the receptor with a variety of diseases, extending from skin problems such as psoriasis and acne, to cancer and metabolic diseases such as diabetes and obesity (8). In the case of diabetes, rexinoids may reduce insulin resistance (3). Also, its role in cell proliferation and apoptosis makes RXR a potential target for cancer research.

The LBD of RXRα forms homodimers and homotetramers in a concentration dependent manner, and addition of the ligand 9-cis-retinoic acid converts the tetramers into dimers regardless of concentration (9). Egea et al. (9) also showed that RXRα/RARα hetereodimers become more compact as 9cRA is bound, with the fully liganded dimer having the most compact structure. The crystal structure of the LBD homodimer of human RXRα (10) was the first reported structure for the RXR family, and it was also the first structure of a nuclear receptor LBD. Following the report of this structure, many other structures of RXR have been determined which include the RXRα LBD in tetrameric form (11), RXRγ LBD bound to all-trans retinoic acid (12), RXRα LBD homodimer bound to 9cRA (13), unliganded RXRα/RARα heterodimer (14), and a variety of homo and heterodimeric structures bound to other natural and synthetic agonists and antagonists, as well as co-activator peptides. RXRα LBD contains 12 alpha

helices and a small beta sheet region. The ligand binding site is buried in a hydrophobic environment located between the β sheet and helices 3, 5, 11, and 12. Binding of the ligand causes a conformational change in the protein described as a 'mousetrap' mechanism in which the final structure has helix 12 closing the binding pocket and trapping the ligand (3, 12).

Although the hRXRα LBD 3-dimensional structure has been previously characterized by crystal structures as mentioned earlier, little is known about the dynamics of the protein in solution. Hydrogen/Deuterium exchange of hRXRα LBD (15) results of 9cRA binding confirm the results observed in the crystal structures. However, residues in helices 7, 10 and 11, as well as in the H7-H8 and H10-H11 loops were unexpectedly shown to be protected, even though they are not directly in contact with the bound 9cRA. Additionally, global unfolding of RXR (1), as determined by circular dichroism and fluorescence emission, revealed that unfolding of the protein follows a minimal three state model with at least one monomeric intermediate.

Human RXRα LBD contains four cysteine residues located along positions C269, C369, C404, and C432. None of these residues is involved in disulfide bonds as confirmed by the crystal structure. These four residues are spatially situated in different regions of the protein and under differing environments, which suggests that solvent accessibility as well as reactivity is expected to be unique for each cysteine. The reactivity of these residues can be measured by the rate of modification with the compound 5,5'-Dithio-bis(2-nitrobenzoic acid) (DTNB), as observed by the production of 2-nitro-5-thiobenzoic acid (TNB) which strongly absorbs light at 412 nm. Analysis of the simultaneous modification of the four cysteines present in the hRXRα LBD may not

allow discerning of the different rates of reaction if some of the phases are close in magnitude. Mutation of some of the cysteine residues can be used to independently study the rates of alkylation for each one. In the present study four mutants were created each containing only a single cysteine and the other cysteine residues were mutated to alanine as it is a good stearic analog. Because the mutation of these residues may affect the 3-dimensional structure of the protein, structural analyses of each hRXRα LBD mutant is important in assessing the validity of the results. Two methods were presently used to assess the structural changes: circular dichroism and fluorescence emission. Since RXR is mostly alpha – helical, circular dichroism reveals changes in overall alpha helical content. Parallel to the CD, the fluorescence emission provides information on changes in the environment of the two tryptophan residues present in the protein.

2.3 - Materials and Methods

Guanidine HCl (Ultrol grade) was purchased from Calbiochem. TCEP and DTNB were purchased from Pierce. CHAPS was purchased from Anatrace. Talon Co^{++} resin was purchased from Clonetech. All other chemicals were purchased from Sigma Chemicals.

2.3.1 - Construction and Purification of the hRXRα LBD Wild-type and Mutants

The pET 15b construct containing the hRXRα LBD (T226 to T462) was the generous gift of Pierre Chambon (Institut de Génétique et de Biologie Moléculaire et Cellulaire, Collège de France, Strasbourg, France). Four single-cysteine mutants were made by using the QuickChange™ site-directed mutagenesis kit (Stratagene) and confirmed by sequencing (all mutagenesis work was done by Rosalyn Upson). Each one of the mutants had three out of the four native cysteine residues (C269, C369, C404, and C432) mutated to alanine: MutC269, hRXRα LBD (C369, C404, C432 →A); MutC369,

hRXRα LBD (C269, C404, C432 →A); MutC404, hRXRα LBD (C269, C369, C432 →A); MutC432, hRXRα LBD (C269, C369, C404 →A). Alanine was chosen because it is a good stearic analog of cysteine.

The wild-type hRXRα LBD and the four mutant dimers were purified as described previously (9). Briefly, cells were grown at 37°C until they reached an absorbance (A_{600}) of 0.6 – 0.7, chilled on ice, and induced to synthesize protein by 0.8 M IPTG at 20°C for 4 h. After collection of the cells by centrifugation, cell pellets were lysed by sonication in the presence of protease inhibitors, followed by centrifugation. The supernatant containing the hexaHis tagged protein was equilibrated with Talon Co^{++} resin in extraction/wash buffer (50 mM KH_2PO_4, 0.3 M KCl, pH 7.4), washed with extraction/wash buffer containing 10 mM imidazole, poured into a column, and eluted using a 10 – 400 mM imidazole gradient (in extraction/wash buffer). The His-tag from the eluted protein was removed by thrombin digestion at 4°C (24 – 48 h, 1 unit/mg protein) followed by separation of the multimeric species on an analytical Sephadex S200HR 2x65 cm size exclusion column freshly equilibrated with buffer (50 mM KH_2PO_4, 0.5 M KCl, 0.5 mM CHAPS, 1 mM TCEP, pH 7.4). Only the homodimeric species were used for experiments. Purity of the protein during the various stages of the purification was evaluated by sodium dodecyl sulfate – polyacrylamide gel electrophoresis, and the concentration was determined using the extinction coefficient of 0.58 $(mg/mL)^{-1}cm^{-1}$ at 280 nm (9).

2.3.2 - Preparation of DTNB Solutions

All DTNB solutions were prepared from a stock solution of 1 M DTNB in DMF. The reaction buffers were flushed with a gentle stream of argon for 30 minutes prior to

the addition of DTNB and subsequent reactions in order to minimize oxidation of the thiols by molecular oxygen and any metal ions present (16-18) . The measured buffer to be used was placed on a glass reacti-vial, warmed on a hot plate, and stock DTNB was added while vigorously stirring until all DTNB had completely dissolved.

2.3.3 - Preparation of L-cysteine and Protein Samples

As mentioned above, all reaction buffers were flushed with argon 30 minutes prior to experiments. L-cysteine samples were prepared by subsequent dilution of a freshly prepared stock solution, were rapidly divided into 200 µL aliquots, and frozen in liquid nitrogen until use. All protein stocks were stored in the presence of 1 mM TCEP, a strong reducing agent, in order to prevent oxidation of the cysteine thiols. However, all protein stocks were additionally incubated in the presence of 5 mM β-mercaptoethanol for 30 – 45 min on ice prior to experiments. Reducing agents were removed using a 5 mL HiTrap (GE Healthcare) desalting column, and protein elution using a 50 mM KH_2PO_4, 0.5 M KCl, 0.5 mM CHAPS, 1 mM EDTA, pH 7.4 buffer was monitored at 280 nm using a Uvicord SII spectrophotometer. Quickly after removal of the reducing agents, the protein concentration was estimated by absorbance at 280 nm using the previously mentioned extinction coefficient, $\varepsilon_{280} = 0.58\ (mg/mL)^{-1}cm^{-1}$, divided into aliquots of 133 or 200 µL, and frozen in liquid nitrogen until use. For each experiment involving protein samples, the addition of 40 ppm Antifoam B (an active silicone emulsion) proved to be critical in reducing foaming of the samples and formation of micro-bubbles in the cuvette after mixing.

2.3.4 - Transient Kinetics Experiments

Stopped flow experiments were carried out using a Biologic SFM-4 stopped-flow spectrophotometer. The temperature was maintained at 30°C using a circulating water bath. The estimated dead-time after mixing the solutions ranged from 2.8 to 5 ms depending on the drive sequence used. A 150 W mercury/xenon lamp with a 1 mm slit width provided the monochromatic light at 412 nm that passed through the sample. For each experiment 3 to 10 kinetic traces, with 2001 to 4001 data points per trace, were averaged. Each kinetic trace followed the appearance of TNB as unreacted thiols were alkylated by DTNB. The reactivity of the amino acid L-cysteine with DTNB was measured in two different sets of experiments. In the first set, [L-cysteine] remained constant and [DTNB] was varied; 80 µL of 13 µM L-cysteine in buffer A (50 mM KH_2PO_4, 0.5 mM CHAPS, 1 mM EDTA, pH 7.4) were mixed with 80 µL of each one of the DTNB solutions (also in buffer A), ranging from 0.65 to 14.3 mM. In the second set of experiments, both [L-cysteine] and [DTNB] remained constant while the denaturant guanidine HCl was increasingly added; 80 µL of 13 µM L-cysteine were mixed with 80 µL of 0.65 mM DTNB, both solutions in buffer A, and in each experiment [GuHCl] was increased from 0 to 5 M in 0.2 M increments. This second set of reactions was repeated using 2.6 mM and 6.5 mM DTNB. The final concentration of L-cysteine was 6.5 µM for all reactions. The final concentrations of DTNB were 0.325 mM, 1.3 mM, and 3.25 mM.

The experiments for the single-cysteine mutants were carried out similarly to the second set of L-cysteine. Both the protein and DTNB concentrations remained constant while GuHCl was increased. For each mutant, 40 µL of protein were mixed with 40 µL of DTNB, both solutions in buffer A (0.5 M KCl was added to the buffer at 0 M GuHCl in

order to stabilize the protein in solution), [GuHCl] was increased from 0 to 5 M in 0.2 M increments for each experiment, and each set of experiments repeated using three different DTNB concentrations ranging from 0.43 to 5.09 mM. The final DTNB concentrations were between 0.216 and 2.54 mM, and the final protein concentrations were between 4.3 and 6.1 μM depending on the mutant.

The wild-type hRXRα LBD was used in two experiments. In the first one, 40 μL of 11.1 μM protein were mixed with 40 μL of 2.22 mM DTNB, both in buffer (0.5 M KCl, 50 mM KH_2PO_4, 0.5 mM CHAPS, 1 mM EDTA, pH 7.4), to give final concentrations of 5.6 μM protein and 1.11 mM DTNB. For the second experiment the DTNB concentration was increased to 5.56 mM DTNB, which made the final DTNB conc. 2.78 mM.

2.3.5 - Circular Dichroism and Fluorescence Spectra

Fluorescence emission spectra were collected with an SLM-Aminco 8000 spectrofluorometer. Samples were excited at 280 nm, and emission intensities were collected from 305 to 550 nm in 1 nm intervals with an integration time of 1 s/nm. All fluorescence intensities were recorded as the ratio of emitted counts to counts from a fraction of the excitation beam scattered from ddIH_20.

Circular dichroism spectra were acquired on a Jasco J-720 spectropolarimeter. Each spectra consisted of an average of ten replicate scans from 440 to 204 nm in 1 nm intervals with an integration time of 1 s/nm. All CD and fluorescence spectra had the background subtracted, and were corrected for baseline shifts.

2.3.6 - Data Analysis

Each kinetic trace was baseline corrected and fitted to a monoexponential function

$$A_{412} = B\left(1 - e^{k_{obs}t}\right) \quad (1)$$

using the Levenberg-Marquardt algorithm. More complex models with additional exponential parameters were rejected on the basis of *F* tests (19, 20) and comparisons of the residuals with the simpler model. Fitting of the the wild-type kinetic traces was piece-wise in order to separate the slow and fast-reacting phases. Additional exponential parameters were required to analyze the data correctly:

$$A_{412} = D_0 - D_1 e^{k'_{obs}t} - D_2 e^{k''_{obs}t} \quad (2)$$

The observed rates of reaction for the L-cysteine experiments were analyzed according to a two-step kinetic mechanism:

$$\text{Cys} + \text{DTNB} \overset{\xi}{\rightleftharpoons} \text{Cys} - \text{DTNB} \overset{k_c}{\rightarrow} \text{Cys} - \text{TNB} + \text{TNB} \quad (3)$$

Under conditions where [DTNB] is in excess over [L-cysteine], formation of the products was assumed to be irreversible. This kinetic model predicts a monoexponential equation for the appearance of products (eq. 1) and a hyperbolic behavior for the observed rates of reaction (see appendix 1 for derivation):

$$k_{obs} = \frac{k_c[\text{DTNB}]}{\xi + [\text{DTNB}]} \quad (4)$$

where $\xi = \frac{(L)(X_2)}{L - X_2}$ represents the pre-equilibrium constant, and k_c represents the reaction rate as [DTNB] approaches saturation. Both k_c and ξ were calculated from the obtained k_{obs} using double reciprocal plots. The effect of GuHCl on k_c and ξ was taken into

account using the following empirical equations, assuming that the equilibrium in the association of DTNB and L-cysteine obeys the linear extrapolation model (21):

$$\xi = e^{\left\{\frac{\alpha-\beta[\mathrm{GuHCl}]}{RT}\right\}} \tag{5}$$

$$k_c = k_c(0)e^{-\gamma[\mathrm{GuHCl}]} \tag{6}$$

Where α, β, and γ are empirical constants and $k_c(0)$ is the maximum rate of reaction in the absence of GuHCl. The parameters obtained from fitting k_c to eq. 6 were used to generate normalization factors for the reaction rates, k_{obs}, of the hRXRα LBD mutants.

Reaction rates for the alkylation of the cysteine residues in the hRXRα LBD mutants were corrected using the normalization factors calculated from the L-cysteine data. The corrected values were then analyzed using a kinetic model in which each protein thiol switches between a closed, P_c, and an open, P_o, conformation, both conformations can form intermediates with [DTNB], but only the $P_o - [\mathrm{DTNB}]$ intermediate undergoes formation of the products (adapted from (22)):

$$\begin{array}{ccccc} P_c + \mathrm{DTNB} & \overset{K}{\rightleftharpoons} & P_o + \mathrm{DTNB} & & \\ \xi \uparrow\downarrow & & \uparrow\downarrow \xi & & \\ P_c\text{–}\mathrm{DTNB} & \underset{K}{\rightleftharpoons} & P_o\text{–}\mathrm{DTNB} & \overset{k_f}{\rightarrow} & P_o\text{–}\mathrm{TNB} + \mathrm{TNB}^{2-} \end{array} \tag{7}$$

Under conditions where [DTNB] is in excess over [hRXRα LBD mutant], formation of the products was assumed to be irreversible. This kinetic model predicts a monoexponential equation for the appearance of products (eq. 1) and a hyperbolic behavior for the observed rates of reaction (see appendix 2 for derivation):

$$k_{obs} = \frac{k'_f[\mathrm{DTNB}]}{\xi + [\mathrm{DTNB}]} \tag{8}$$

where k'_f, the reaction rate as [DTNB] approaches saturation, is given by:

$$k'_f = \frac{k_f K}{K+1} \tag{9}$$

and $\xi = \frac{(P_o)(\mathrm{DTNB})}{P_o\text{–DTNB}} = \frac{(P_c)(\mathrm{DTNB})}{P_c\text{–DTNB}}$ is the pre-equilibrium constant, and $K = \frac{P_o}{P_c} = \frac{P_o\text{–DTNB}}{P_c\text{–DTNB}}$ is the closing – opening rate of each thiol. The model in eq. 7 also predicts the effects of the denaturant GuHCl on the system, as the free energy of the reaction is given by (assuming that the equilibrium in the association of DTNB and each protein thiol obeys the linear extrapolation model (21))

$$\Delta G^\circ = \Delta G^\circ(\mathrm{H_2O}) - m[\mathrm{GuHCl}] = -RT\ln K \tag{10}$$

$$K = e^{\left\{\frac{m[\mathrm{GuHCl}] - \Delta G^\circ(\mathrm{H_2O})}{RT}\right\}} \tag{11}$$

where $\Delta G^\circ(\mathrm{H_2O})$ is the free energy of the reaction in the absence of GuHCl, and m, the cooperativity constant, gives the GuHCl dependence. The midpoint of the transition is given by $\Delta G^\circ(\mathrm{H_2O})/m$.

All the data presented here was fitted and graphed using the open-source program QtiPlot 0.9-rc2 (http://soft.proindependent.com/qtiplot.html), except for the GuHCl titrations of the hRXRα LBD mutants which were weighted by $1/\sigma^2$ (20) and fitted with the program Scientist (Micromath Scientific Software, Salt Lake City, UT) .

2.4 - Results

2.4.1 - L-Cysteine

The hyperbolic behavior of the reaction between L-cysteine and DTNB is illustrated in Fig. 1. Fitting of these data to equation 1 yielded a maximum rate of reaction of k_c= 16.6 ± 1.0 s^{-1} and a pre-equilibrium constant of ξ = 2.47 ± 0.40 mM Although the author could find little information in the literature regarding the two-step mechanism for the alkylation of cysteine thiols by DTNB, Chase (22) found similar results to the ones presented here.

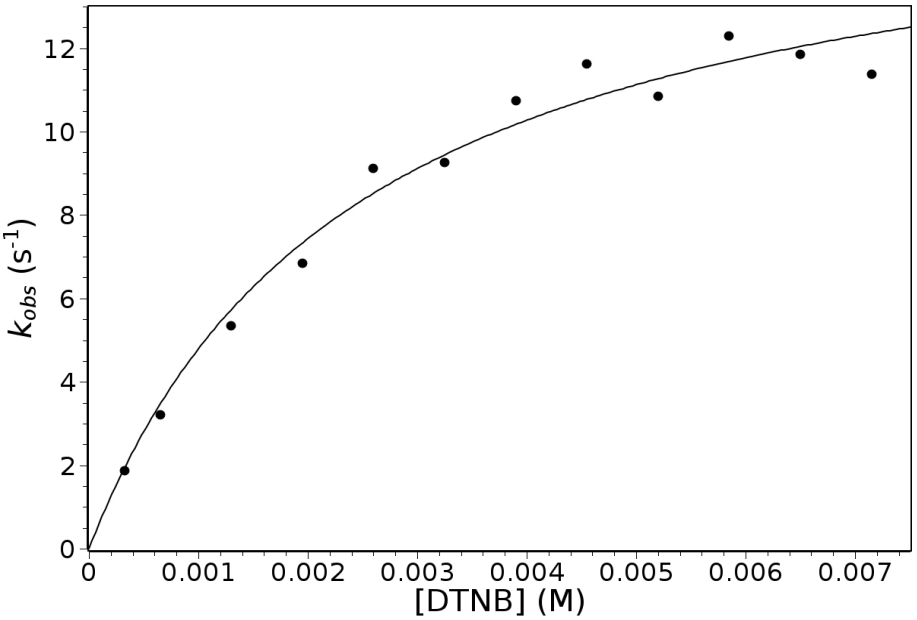

Figure 1. Observed rates of reaction of 6.5 μM L-cysteine with increasing concentrations of DTNB fitted to eq. 4: k_c= 16.6 ± 1.0 s^{-1} and ξ = 2.47 ± 0.40 mM.

The pK_a of the cysteine thiol is affected by the presence of GuHCl, which in turn alters the observed rates of reaction (Fig. 2). This effect on the pK_a has been studied for other amino acid side chains (23, 24). A significant leap in the rate of reaction was

observed going from 0 to 0.2 M GuHCl at all concentrations of DTNB. As the concentration of GuHCl is continuously increased, the rates fall dramatically.

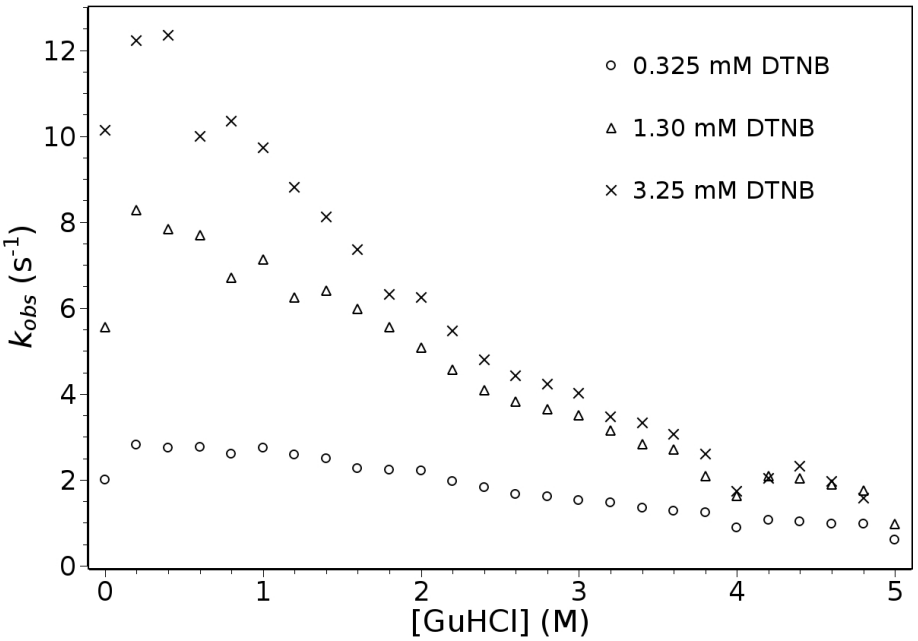

Figure 2. Observed rates of reaction, k_{obs}, of L-cysteine (6.5 μM) with three different concentrations of DTNB (0.325 mM, 1.30 mM, and 3.25 mM) in the presence of increasing concentrations of GuHCl.

The observed rates of reaction (Fig. 2) were fitted to the two-step mechanism, eq. 3, using eq. 4 as described in the Materials and Methods section. Results from this fitting (Fig. 3) provide the maximum rates, k_c (Fig. 3), and pre-equilibrium constants, ξ (Fig. 4), for the alkylation of L-cysteine by DTNB at each concentration of GuHCl. The empirical equations 5 and 6 describe the behavior of ξ and k_c well, and provide the parameters needed to generate the normalization factors used to correct the mutant reaction rates.

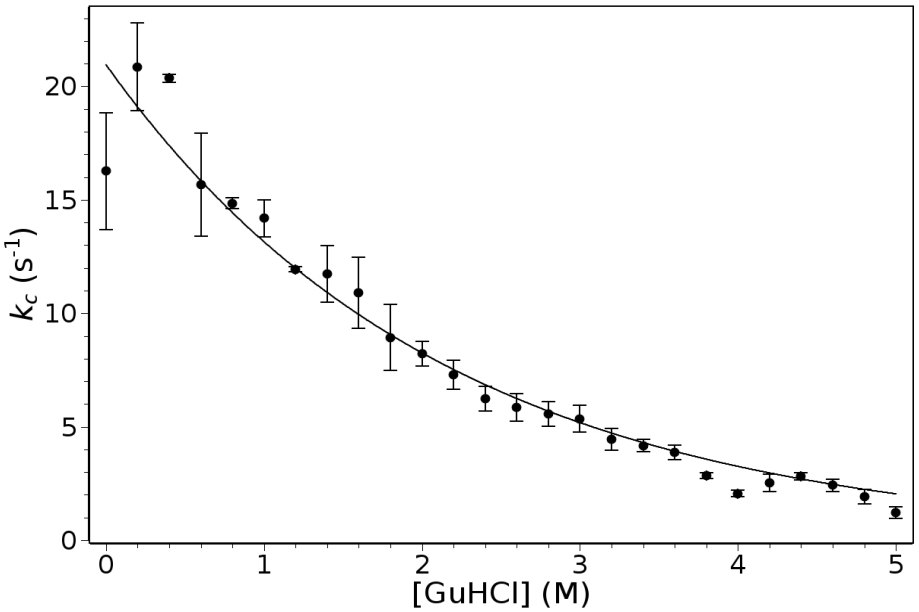

Figure 3. Maximum rates of alkylation, k_c, of L-cysteine by DTNB in the presence of GuHCL. Data fitted to eq. 6: $k_c(0) = 20.95 \pm 0.75$ s^{-1} and $\gamma = 0.466 \pm 0.026$ M^{-1}.

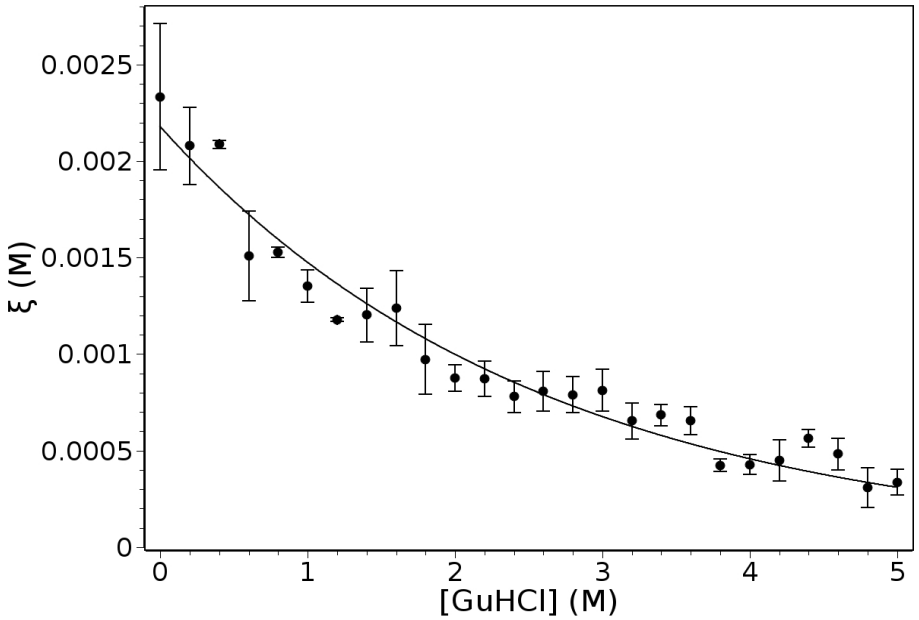

Figure 4. Pre-equilibrium constants, ξ, for the alkylation of L-cysteine by DTNB in the presence oh GuHCl. Data fitted to eq. 4: $\alpha = -3{,}693 \pm 17$ cal/mol and $\beta = 234.7 \pm 11.4$ cal/mol·M.

2.4.2 - hRXRα LBD Mutants

A sample of the kinetic traces obtained from the DTNB alkylation of the hRXRα LBD mutants is shown in Fig. 5. The apparent concentration of thiols seen in all of the kinetic traces varied from 30 to 70% of the estimated protein concentration, as calculated from the observed change in absorbance: conc. of unreacted thiols = [TNB] = $\Delta A_{412}/\varepsilon_{412}$ (ε_{412} = 14,150 M^{-1} cm^{-1} in buffer and ε_{412} = 13,700 M^{-1} cm^{-1} in the presence of 6 M GuHCl (18)). This discrepancy between the observed and the expected number of free thiols may be due to several reasons which include oxidation by O_2 and metal ions, inability of reducing agents to access buried cysteine residues, and overestimation of the protein concentration calculated from the A_{280}.

The maximum rate of reaction of MutC269 in the absence of GuHCl, k'_f = 17.3 ± 3.6 s^{-1}, is very close to the value for L-cysteine, 16.6 ± 1.0 s^{-1}, which may indicate that residue C269 is fully accessible under native conditions. Addition of 1 M GuHCl to the reaction more than tripled the initial value of k'_f (Fig. 6), yet it rapidly returned to the initial value at higher GuHCl concentrations.

Alkylation of MutC369 was very slow under native conditions, giving a maximum rate of reaction of k'_f = 0.0187 ± 0.0022 s^{-1}. Titration with GuHCl (Fig. 7) showed that k'_f rapidly began to increase after 1.4 M GuHCl and continued to rise until it reached 2.2 M GuHCl, point at which it became steady. Fitting of the unfolding transition of MutC369 to the model proposed in eq. 7, using equations 9 and 11, produced the following parameters: m = 3,230 ± 330 cal/mol·M, $\Delta G^o(H_2O)$ = 5,380 ± 560 cal/mol, k_f = 20.7 ± 2.2 s^{-1}. The midpoint of this unfolding transition ($\Delta G^o(H_2O)$/m) was calculated to be 1.67 ± 0.24 M GuHCl.

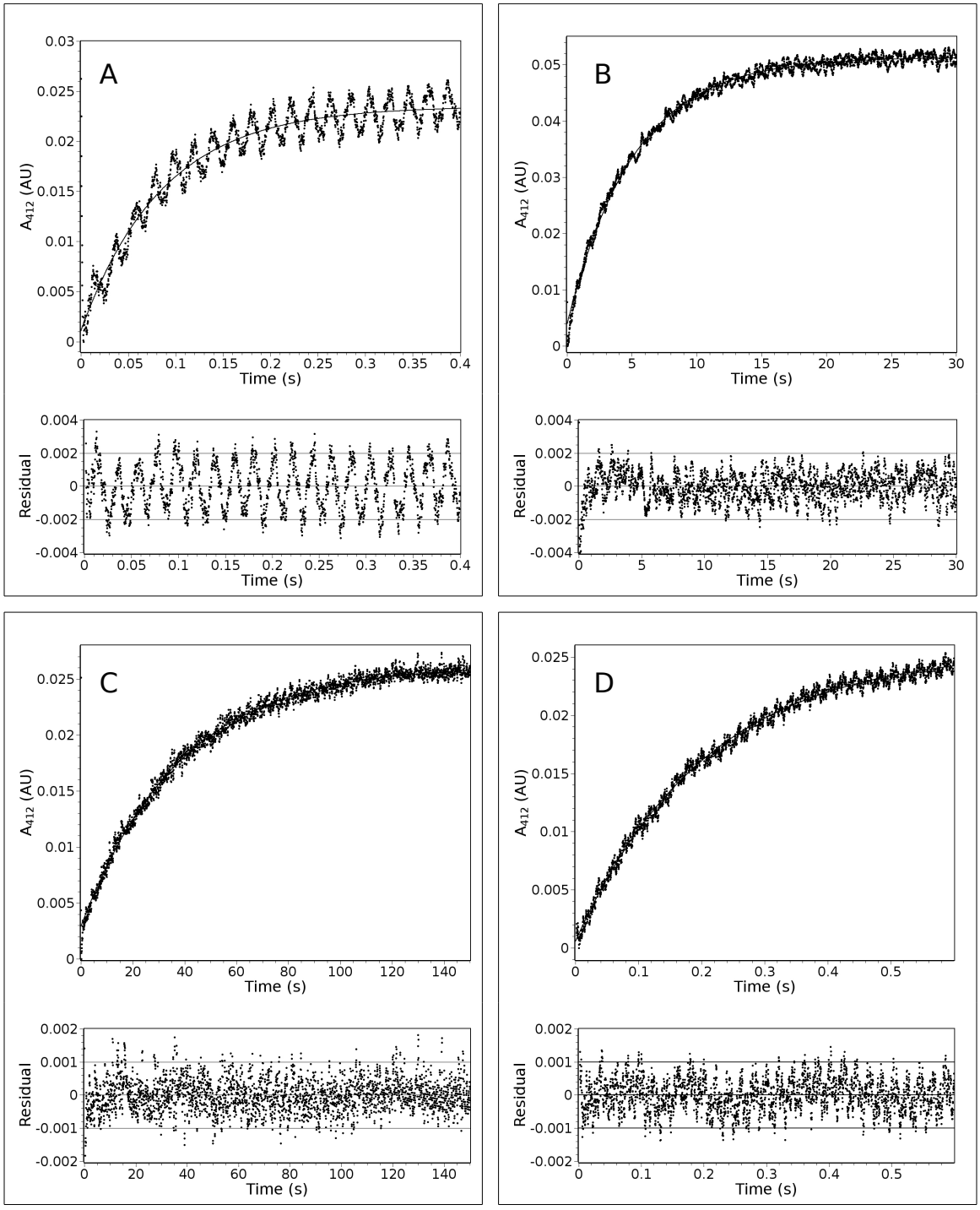

Figure 5. Sample kinetic traces of the four different hRXRα LBD mutants fitted to equation 1. (A) 5.1 μM MutC269, 2.54 mM DTNB, no GuHCl. $\Delta A_{412} = 0.0224$, k_{obs}=11.63 s^{-1}. (B) 5.2 μM MutC369, 1.80 mM DTNB, 1.2 M GuHCl. $\Delta A_{412} = 0.0474$, k_{obs}=0.1945 s^{-1}. (C) 4.3 μM MutC404, 0.864 mM DTNB, 1.0 M GuHCl. $\Delta A_{412} = 0.0233$, k_{obs}=0.02627 s^{-1}.(D) 4.0 μM MutC432, 0.802 mM DTNB, 2.2 M GuHCl. $\Delta A_{412} = 0.0250$, k_{obs}=4.83 s^{-1}. Residuals shown underneath each trace.

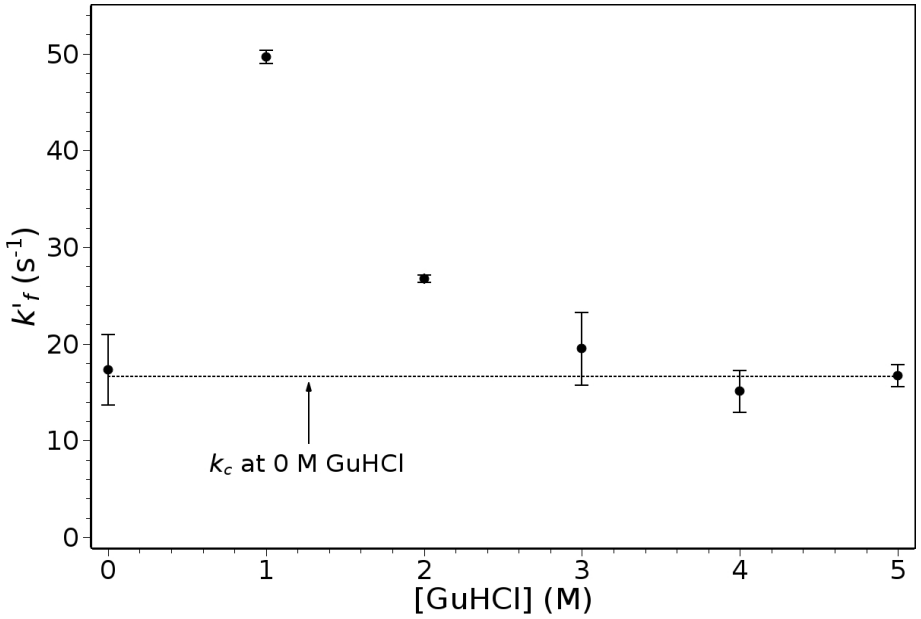

Figure 6. Titration of MutC269 with GuHCl. Maximum rates of reaction, k'_f, were obtained from fitting the corrected (using L-Cys normalization factors) observed rates of reaction, k_{obs}, to eq. 8.

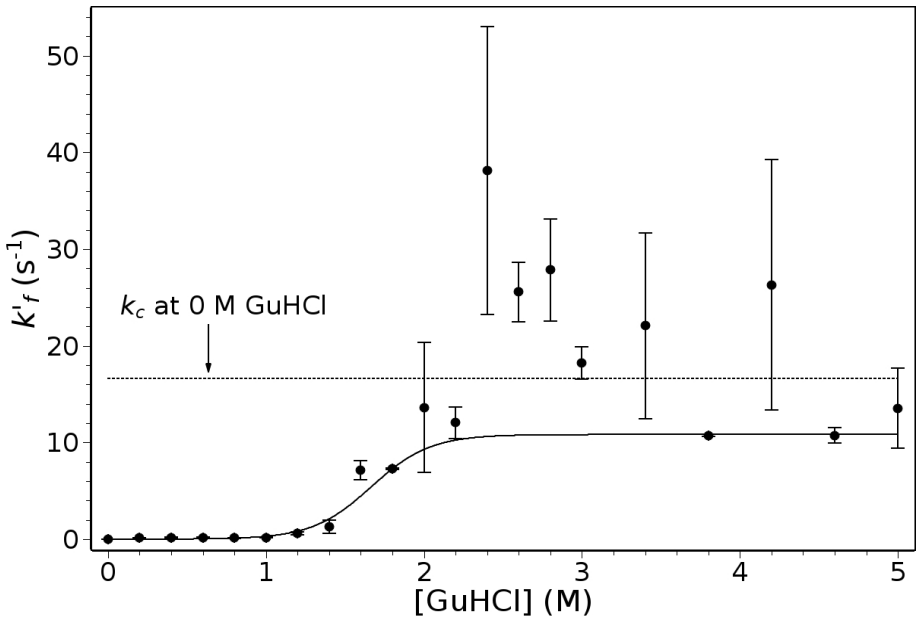

Figure 7. Titration of MutC369 with GuHCl. Maximum rates of reaction, k'_f, were obtained from fitting the corrected (using L-Cys normalization factors) observed rates of reaction, k_{obs}, to eq. 8. Unfolding transition fitted using equations 9 and 11: m = 3,230 ± 330 cal/mol·M, $\Delta G^{o}(H_2O)$ = 5,380 ± 560 cal/mol, k_f = 10.8 ± 0.4 s^{-1}.

The behavior of MutC404 in the absence of GuHCl was similar to MutC369, yet even slower, showing a maximum rate of reaction of $k'_f = 0.00089 \pm 0.00023$ s^{-1}. Titration with GuHCl (Fig. 8) showed that k'_f started to rapidly increase after 1.4 M GuHCl and it continued to do so until it reached 3.4 – 3.6 M GuHCl. This unfolding transition extended over a broader GuHCl concentration than the transition for MutC369 did. Fitting of the unfolding transition of MutC404 to the model proposed in eq. 7, using equations 9 and 11, produced the following parameters: m = 2,310 ± 150 cal/mol·M, $\Delta G^o(H_2O)$ = 5,300 ± 350 cal/mol, k_f = 14.8 ± 0.1 s^{-1}. The midpoint of this unfolding transition ($\Delta G^o(H_2O)$/m) was calculated to be 2.29 ± 0.21 M GuHCl.

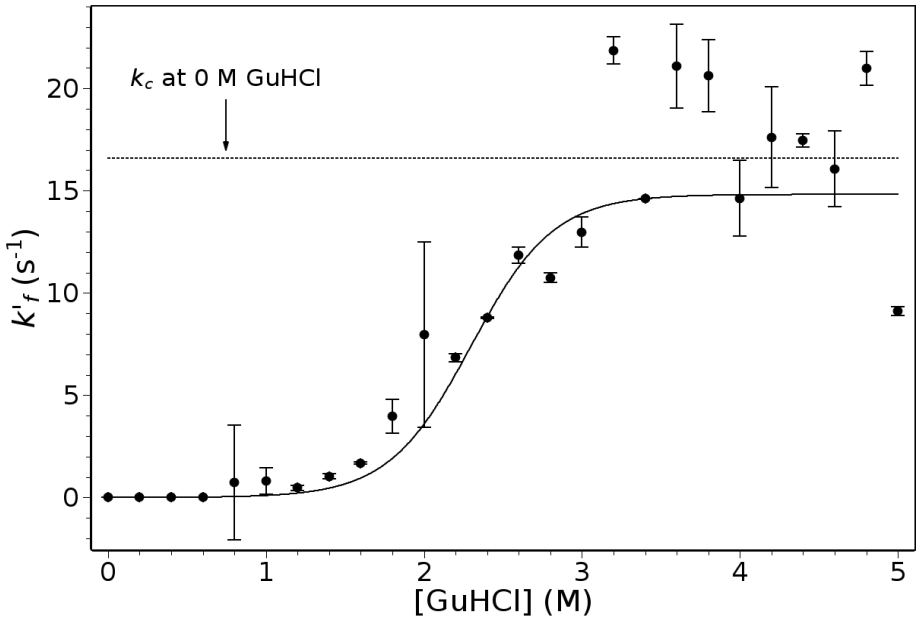

Figure 8. Titration of MutC404 with GuHCl. Maximum rates of reaction, k'_f, were obtained from fitting the corrected (using L-Cys normalization factors) observed rates of reaction, k_{obs}, to eq. 8. Unfolding transition fitted using equations 9 and 11: m = 2,310 ± 150 cal/mol·M, $\Delta G^o(H_2O)$ = 5,300 ± 350 cal/mol, k_f = 14.8 ± 0.1 s^{-1}.

The last mutant, MutC432, showed a maximum rate of alkylation k'_f = 2.01 ± 0.018 s^{-1}in the absence of GuHCl, which is significantly faster than the rate of MutC369

and MutC404, yet slower than the rate of MutC269. As with the previous two mutants, titration with GuHCl (Fig. 9) showed that k'_f started to rapidly increase this time after 1.0 M GuHCl and it continued to do so until it reached 2.4 M GuHCl. This unfolding transition began at a lower GuHCl concentration than the transitions for MutC369 and MutC404. Fitting of the unfolding transition of MutC432 to the model proposed in eq. 7, using equations 9 and 11, produced the following parameters: m = 1,170 ± 210 cal/mol·M, ΔGº(H2O) = 1,780 ± 170 cal/mol, k_f = 15.8 ± 1.6 s^{-1}. The midpoint of this unfolding transition ($\Delta G^o(H_2O)$/m) was calculated to be 1.52 ± 0.31 M GuHCl.

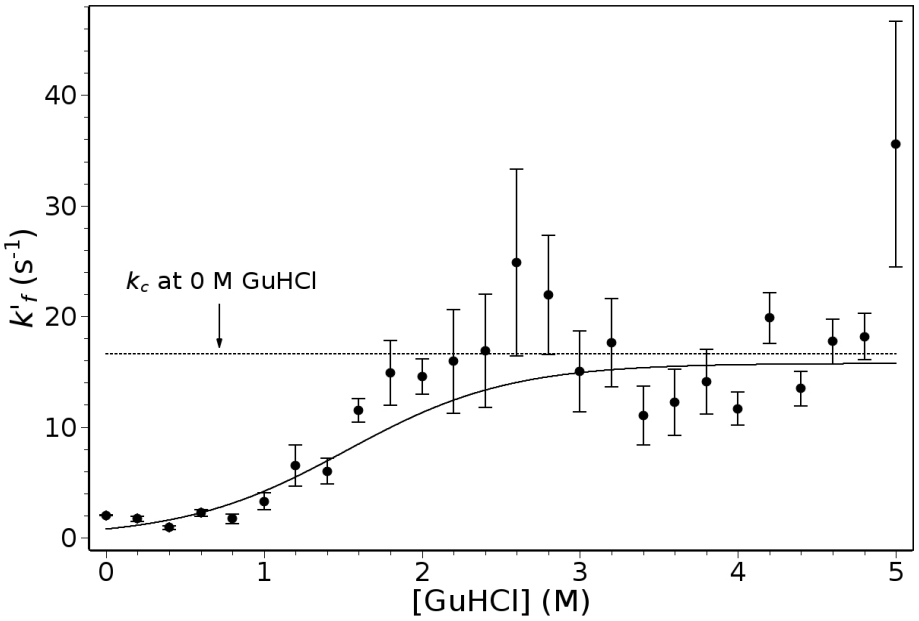

Figure 9. Titration of MutC432 with GuHCl. Maximum rates of reaction, k'_f, were obtained from fitting the corrected (using L-Cys normalization factors) observed rates of reaction, k_{obs}, to eq. 8. Unfolding transition fitted using equations 9 and 11: m = 1,170 ± 210 cal/mol·M, $\Delta G^o(H_2O)$ = 1,780 ± 170 cal/mol, k_f = 15.8 ± 1.6 s^{-1}.

The unfolding parameters obtained for MutC369, MutC404, and MutC432 are summarized in Table 1.

Table 1. Summary of the thermodynamic parameters obtained from the unfolding titrations of MutC369, MutC404, and MutC432.

Protein	m (cal/mol·M)	$\Delta G^{o}(H_2O)$ (cal/mol)	k_f (s^{-1})	Transition Midpoint (M GuHCl)
MutC369	3,230 ± 330	5,380 ± 560	10.8 ± 0.4	1.67 ± 0.24
MutC404	2,310 ± 150	5,300 ± 350	14.8 ± 0.1	2.29 ± 0.21
MutC432	1,170 ± 210	1,780 ± 170	15.8 ± 1.6	1.52 ± 0.31
		L-cysteine k_c	16.6 ± 1.0	

2.4.3 - Alkylation of the hRXRα LBD Wild-type

Alkylation of the wild-type hRXRα LBD was divided into a slow (over 30 minutes) and a fast region (less than a minute) as shown in Fig. 10.

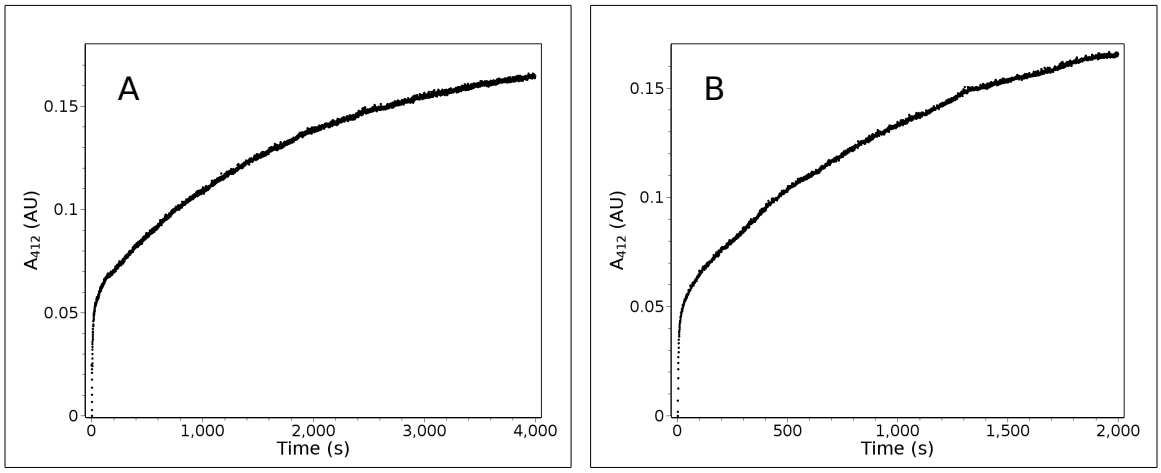

Figure 10. Alkylation of the wild-type hRXRα LBD by DTNB under native conditions. (A) 5.6 μM hRXRα LBD and 1.11 mM DTNB. (B) 5.6 μM hRXRα LBD and 2.78 mM DTNB.

Further examination of the fast region (Fig. 11A and 12A) indicated that two fast kinetic phases take place very rapidly. Analysis of the data in this region to a bi-exponential model (eq. 2) showed two phases of similar amplitude and alkylation rates

comparable to those of MutC269 and MutC432 (Table 2). The slow region (Fig. 11B and 12B) proved to be more challenging to analyze, as the fitting software was unable to fit this region to a bi-exponential model (assuming that the reaction rates are different). This slow region was then analyzed using a mono-exponential model (eq. 1), which produced an observed change in absorbance of roughly the same amplitude as the change in absorbance of the fast region (Table 2). In addition to this, the rate of reaction is within the same order of magnitude as the rates for MutC369 and MutC404 (Table 2).

Table 2. Reaction rates obtained from the alkylation of the hRXRα LBD wild-type compared to those of the mutants.

[DTNB]	Protein Species	D_1 (AU)	D_2 (AU)	k'_{obs} (s^{-1})	k''_{obs} (s^{-1})	B (AU)	k_{obs} (s^{-1})
1.11 mM	Wild-Type	0.0371	0.0596	7.17	0.173	0.119	0.000562
	Mutants	–	–	6.36[a]	0.484[b]	–	0.00135[c] 0.000214[d]
2.78 mM	Wild-Type	0.0365	0.0578	10.7	0.310	0.134	0.000934
	Mutants	–	–	10.3[a]	0.890[b]	–	0.00305[c] 0.000393[d]
	Expected ΔA_{412}/Cys	0.0792					

[a] k_{obs} for MutC269
[b] k_{obs} for MutC432
[c] k_{obs} for MutC369
[d] k_{obs} for MutC404

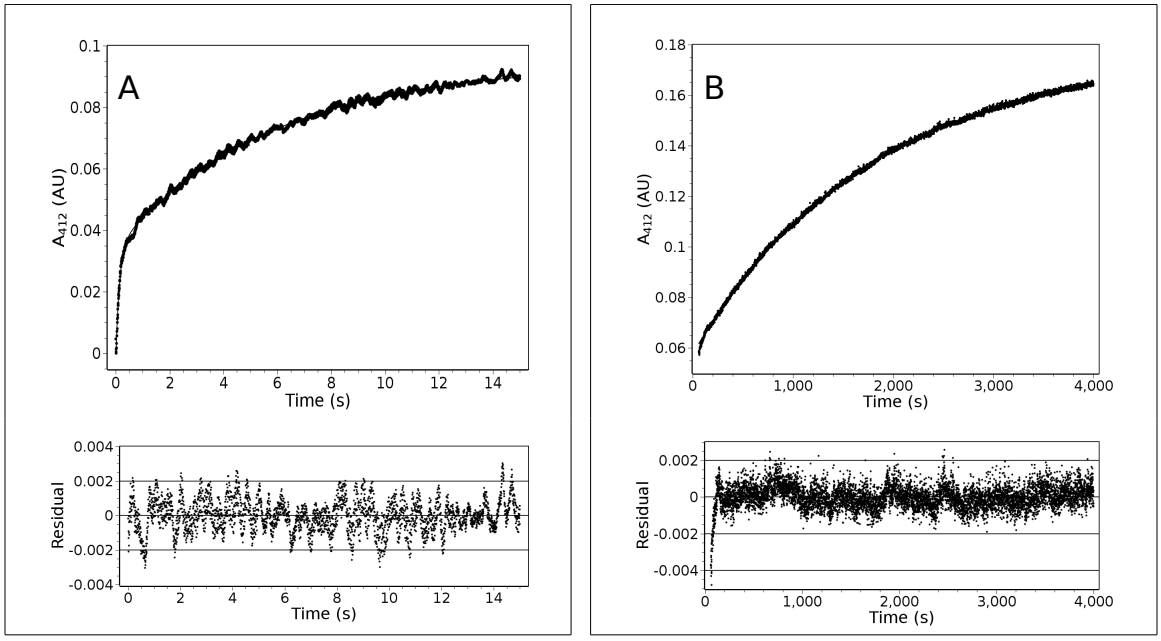

Figure 11. Alkylation of the wild-type hRXRα LBD by DTNB under native conditions. 5.6 μM hRXRα LBD and 1.11 mM DTNB. (A) Fast region fitted to eq. 2: D_1 = 0.0371 ± 0.0004 AU, D_2 = 5.96 ± 0.08 E-2 AU, k'_{obs} = 7.17 ± 0.12 s^{-1}, k''_{obs} = 0.173 ± 0.001 s^{-1}. (B) Slow region fitted to eq. 1: B = 0.11900 ± 0.00004 AU, k_{obs} = 0.000562 +/- 0.000001 s^{-1}.

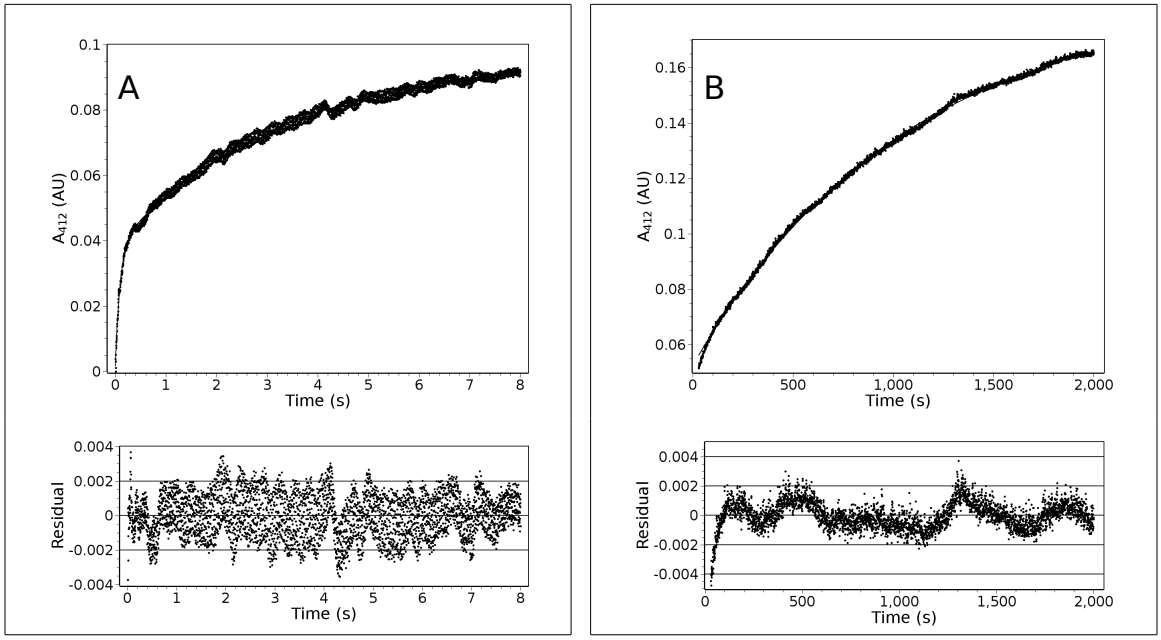

Figure 12. Alkylation of the wild-type hRXRα LBD by DTNB under native conditions. 5.6 μM hRXRα LBD and 1.11 mM DTNB. (A) Fast region fitted to eq. 2: D_1 = 0.0365 ± 0.0004 AU, D_2 = 0.0578 ± 0.0001 AU, k'_{obs} = 10.7 ± 0.2 s^{-1}, k''_{obs} = 0.310 ± 0.002 s^{-1}, (B) Slow region fitted to eq. 1: B = 0.1340 ± 0.0001 AU, k'_{obs} = 0.000934 ± 0.000002 s^{-1}.

2.4.4 - Circular Dichroism and Fluorescence Emission Spectra

Circular dichroism and fluorescence emission were measured in order to provide a qualitative estimate of the structural changes incurred due to the mutations in the used proteins.

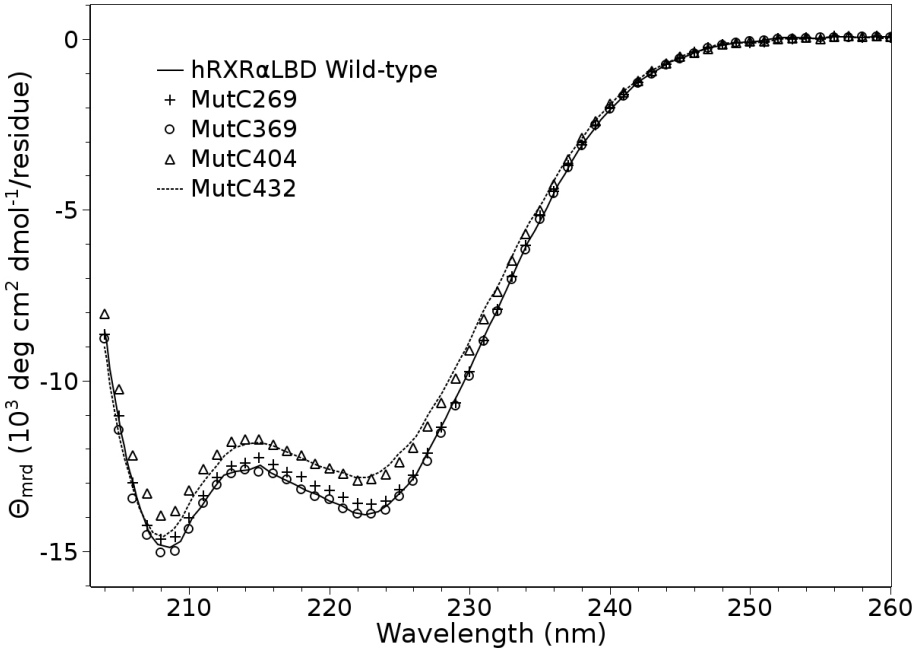

Figure 13. Molar ellipticities per residue of the hRXRα LBD wild-type and the four hRXRα LBD mutants.

The molar ellipticities per residue (Fig. 13) of MutC269 and MutC369 follow the values of the wild-type closely. On the other hand, The ellipticities for MutC404 and MutC432 seem to deviate significantly from the wild-type. In order discard any possible errors of the concentration measurements, an intensity-weighted average wavelength

$$\overline{\lambda} = \frac{\sum I_i \lambda_i}{\sum I_i} \tag{12}$$

was calculated for each protein species and the results shown in Table 3. The calculated CD intensity-weighted average wavelength of MutC432 is 3.49 nm higher than the value

of the wild-type, a considerably higher deviation compared to the other mutants: 0.07 nm for MutC269, 1.09 nm for MutC369, and 0.89 nm for MutC404.

Table 3. Intensity – weighted average wavelengths for fluorescence emission and circular dichroism of the wild-type hRXRα LBD and the four mutants.

	Wild-Type	MutC269	MutC369	MutC404	MutC432
CD	215.79	215.72	216.88	216.68	219.28
Fluorescence	348.51	348.80	348.62	348.92	348.16

The concentration-corrected fluorescence emissions (Fig. 14) show that the spectra for the mutants follows the same shape as the mutant, but the amplitudes vary significantly. Again, intensity-weighted average wavelengths (eq. 12) were calculated for the fluorescence emission each protein species and the results shown in Table 3. Results from this calculation show that the intensity-weighted average wavelengths for the mutants is within 0.5 nm the value for the wild-type.

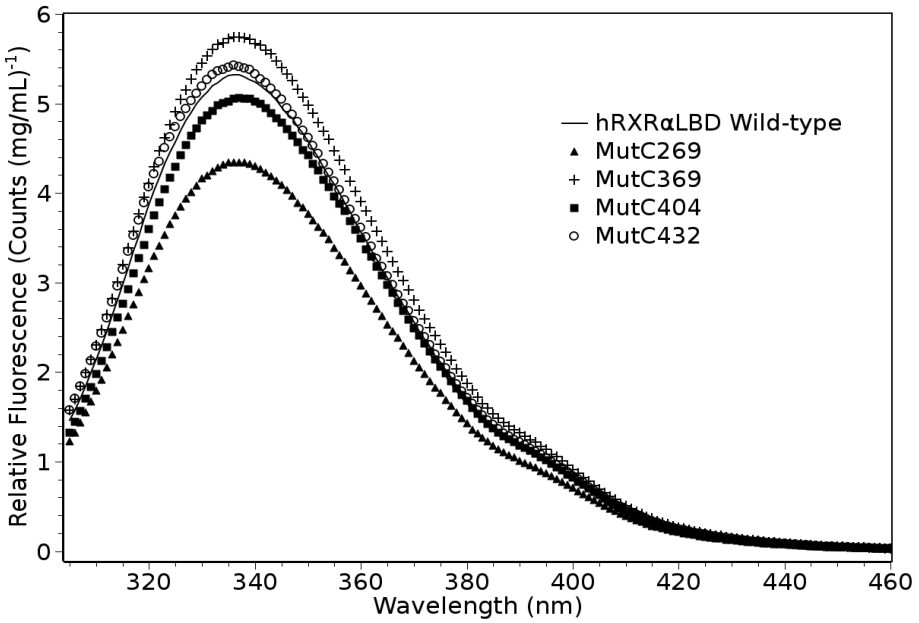

Figure 14. Fluorescence emission of the hRXRα LBD wild-type and the four hRXRα LBD mutants. Excitation wavelength 280 nm.

2.5 - Discussion

Examination of the L-cysteine vs DTNB in the absence and presence of GuHCl was a crucial initial step for the analysis of the subsequent protein experiments. The dependence of the rates of reaction on DTNB concentration (Fig. 1) provided a gauge for the range of values needed to be used in the protein experiments. The GuHCl titration for the free amino acid (Fig. 2) clearly showed that the rates of alkylation are significantly affected by the presence of denaturant, and so this behavior needed to be corrected in order to properly analyze the protein results.

Analytical ultracentrifugation results (data not shown) predict that roughly 70% of the protein form homodimers and 30% remains as monomers at the range of concentrations used. If the reactivity of the cysteine residues were dependent on dimerization, two kinetic phases would be expected for the alkylation by DTNB. However, all the collected spectra obtained from the hRXRα LBD mutants were successfully analyzed using mono-exponential functions (as described in the Methods section), which indicates that the reactivity of the four residues is independent of dimerization. Fitting of the kinetic traces to double-exponential models was rejected after inspection of the residuals as well as comparison using F-tests showed that addition of the second exponential phase did not improve the fitting significantly enough to adopt the more complex model.

Although the GuHCl titration of MutC269 did not provide any information on the unfolding energetics, its agreement with the L-cysteine results supports the use of the free amino acid as a model compound for the alkylation by DTNB. The sudden rise observed at 1 M GuHCl is not understood, but it may be due to a change in the electrostatic

environment of the residue caused by the presence of denaturant. The apparent full accessibility of residue C269 is further supported by previous H/D exchange results (Yan et al., (15)) showing that between 70 to 85% of the backbone amide hydrogens for this residue are exchanged within 15 seconds.

Titration of the three other mutants showed that the unfolding transition for each mutant is different from the other two. The mid-point of all three transitions is well separated and the free energy of unfolding is also different. Residue C432 appears to be the most accessible, followed by C369, and C404 is the least accessible. Again, comparison of these results with previous H/D exchange findings (15), further supports the results found herein as over 85% of the backbone amide hydrogens for residue C432 are exchanged within 60 seconds, and exchange of the backbone amide hydrogens for residue C404 was less than 70% after 30 minutes (no data is presented by Yan et al., (15), for residue C369, but surrounding residues exchanged very slowly). Examination of the crystal structure (10) of hRXRα LBD wild-type reveals that residues C369 and C432 are involved in one hydrogen bond each, and residue C404 is involved in two hydrogen bonds. The latter result helps to account for the broader transition and higher free energy for unfolding of MutC404. Continued consideration of the crystal structure, as well as the amino acid sequence, shows that all the cysteine residues in hRXRα LBD are surrounded by hydrophobic groups (these groups are stabilized by the presence of GuHCl), which in combination with the presented findings support the hypothesis that the observed transitions represent local unfolding rather than a global event. Global unfolding results of hRXRα LBD obtained by Harder et al. (1) further supports this hypothesis as 2.6 – 2.8

M GuHCl is required to unfold 50% of the protein (in the same range of concentrations), which takes place after the midpoint of the three observed transitions.

The results from the circular dichroism and fluorescence emission indicate that the structure of the mutant species is altered differently depending on the residues mutated. Overall, the structure of MutC269 seems to be the least affected by the mutations, while the alpha-helical content of MutC432 was significantly changed.

Analysis of the alkylation of the wild-type hRXRα LBD was a necessary control as to see if the observed rates of reaction for this species agree with the results obtained from the mutants. Three apparent kinetic phases were obtained from the analysis: the fastest phase was in good agreement with MutC269, the middle phase was roughly 2.8 times slower than MutC432, and the last phase appears to be a combination of MutC369 and MutC404. The amplitudes of each phase agree with the expected results. The observed difference between the observed rates of MutC432 and the middle kinetic phase of the wild-type maybe due to structural changes incurred by the mutations, as the alpha-helical content of this mutant may be different from the wild-type.

Chapter 3

Conclusion

Alkylation of cysteine thiols follows a two – step mechanism which is affected by the presence of the denaturant guanidine HCl. The observed reactivities of each of the hRXRα LBD mutants confirmed that the four cysteine residues had differences in accessibility and were in different environments. The obtained thermodynamic parameters for each of the unfolding transitions, as measured by GuHCl titrations of the single – cysteine mutants, suggest that they each represent local unfolding of specific regions of the protein, and not a global unfolding event. Reaction rates of the hRXRα LBD agree with the results obtained from the mutants within error. Changes in the structure determined by CD and fluorescence emission showed that the structure of the mutants may be slightly different than the wild-type, except for MutC432 which may have more significant changes in its alpha-helical content.

BIBLIOGRAPHY

[1] Harder, M.E., Deinzer, M.L., Leid, M.E. & Schimerlik, M.I. Global analysis of three-state protein unfolding data. *Protein Sci* (2004) **13**: pp. 2207-2222.

[2] Chambon, P. A decade of molecular biology of retinoic acid receptors. *FASEB J* (1996) **10**: pp. 940-954.

[3] Laudet, V. & Gronemeyer, H.. The nuclear receptor factsbook. . Academic Press, 2002.

[4] Germain, P., Chambon, P., Eichele, G., Evans, R.M., Lazar, M.A., Leid, M., De Lera, A.R., Lotan, R., Mangelsdorf, D.J. & Gronemeyer, H. International union of pharmacology. lxiii. retinoid x receptors. *Pharmacol Rev* (2006) **58**: pp. 760-772.

[5] Leid, M., Kastner, P. & Chambon, P. Multiplicity generates diversity in the retinoic acid signalling pathways. *Trends Biochem Sci* (1992) **17**: pp. 427-433.

[6] Mader, S., Chen, J.Y., Chen, Z., White, J., Chambon, P. & Gronemeyer, H. The patterns of binding of rar, rxr and tr homo- and heterodimers to direct repeats are dictated by the binding specificites of the dna binding domains. *EMBO J* (1993) **12**: pp. 5029-5041.

[7] Mader, S., Leroy, P., Chen, J.Y. & Chambon, P. Multiple parameters control the selectivity of nuclear receptors for their response elements. selectivity and promiscuity in response element recognition by retinoic acid receptors and retinoid x receptors. *J Biol Chem* (1993) **268**: pp. 591-600.

[8] Thacher, S.M., Vasudevan, J. & Chandraratna, R.A. Therapeutic applications for ligands of retinoid receptors. *Curr Pharm Des* (2000) **6**: pp. 25-58.

[9] Egea, P.F., Rochel, N., Birck, C., Vachette, P., Timmins, P.A. & Moras, D. Effects of ligand binding on the association properties and conformation in solution of retinoic acid receptors rxr and rar. *J Mol Biol* (2001) **307**: pp. 557-576.

[10] Bourguet, W., Ruff, M., Chambon, P., Gronemeyer, H. & Moras, D. Crystal structure of the ligand-binding domain of the human nuclear receptor rxr-alpha. *Nature* (1995) **375**: pp. 377-382.

[11] Gampe, R.T.J., Montana, V.G., Lambert, M.H., Wisely, G.B., Milburn, M.V. & Xu, H.E. Structural basis for autorepression of retinoid x receptor by tetramer formation and the af-2 helix. *Genes Dev* (2000) **14**: pp. 2229-2241.

[12] Renaud, J.P., Rochel, N., Ruff, M., Vivat, V., Chambon, P., Gronemeyer, H. & Moras, D. Crystal structure of the rar-gamma ligand-binding domain bound to all-trans retinoic acid. *Nature* (1995) **378**: pp. 681-689.

[13] Egea, P.F., Mitschler, A., Rochel, N., Ruff, M., Chambon, P. & Moras, D. Crystal structure of the human rxralpha ligand-binding domain bound to its natural ligand: 9-cis retinoic acid. *EMBO J* (2000) **19**: pp. 2592-2601.

[14] Bourguet, W., Vivat, V., Wurtz, J.M., Chambon, P., Gronemeyer, H. & Moras, D. Crystal structure of a heterodimeric complex of rar and rxr ligand-binding domains. *Mol Cell* (2000) **5**: pp. 289-298.

[15] Yan, X., Broderick, D., Leid, M.E., Schimerlik, M.I. & Deinzer, M.L. Dynamics and ligand-induced solvent accessibility changes in human retinoid x receptor homodimer determined by hydrogen deuterium exchange and mass spectrometry. *Biochemistry* (2004) **43**: pp. 909-917.

[16] Bagiyan, G.A., Koroleva1, I.K., Soroka, N.V. & Ufimtsev, A.V. Oxidation of thiol compounds by molecular oxygen in aqueous solutions. *Russian Chemical Bulletin* (2003) **52:5**: pp. 1135-1141.

[17] Riddles, P.W., Blakeley, R.L. & Zerner, B. Reassessment of ellman's reagent. *Methods Enzymol* (1983) **91**: pp. 49-60.

[18] Riddles, P.W., Blakeley, R.L. & Zerner, B. Ellman's reagent: 5,5'-dithiobis(2-nitrobenzoic acid)--a reexamination. *Anal Biochem* (1979) **94**: pp. 75-81.

[19] Motulsky, H.J. & Ransnas, L.A. Fitting curves to data using nonlinear regression: a practical and nonmathematical review. *FASEB J* (1987) **1**: pp. 365-374.

[20] Bevington, P.R.. Data reduction and error analysis for the physical sciences. . McGraw-Hill, 1969.

[21] Schellman, J.A. Solvent denaturation *Biopolymers* (1978) **17**: pp. 1305-1322.

[22] Chase, T.J. Mannitol-1-phosphate dehydrogenase of escherichia coli. chemical properties and binding of substrates. *Biochem J* (1986) **239**: pp. 435-443.

[23] Garcia-Mira, M.M. & Sanchez-Ruiz, J.M. Ph corrections and protein ionization in water/guanidinium chloride. *Biophys J* (2001) **81**: pp. 3489-3502.

[24] Nozaki, Y. & Tanford, C. Acid-base titrations in concentrated guanidine hydrochloride. dissociation constants of the guamidinium ion and of some amino acids. *J Am Chem Soc* (1967) **89**: pp. 736-742.

APPENDICES

Appendix I

Kinetic Equations for the Alkylation of L-cysteine by DTNB

Kinetic Equations for the Alkylation of L-Cysteine by DTNB

$$L + X_2 \overset{\xi}{\rightleftharpoons} L\text{–}X_2 \overset{k_c}{\rightarrow} L\text{–}X + X \qquad \text{(eq. 3)}$$

$X_2 = \text{DTNB}$, $X = \text{TNB}$

$L = \text{L -Cysteine}$

$A_T = \text{Total amount of cystein and derivatives}$

$X_2 \gg A_T$

$$\xi = \frac{(L)(X_2)}{L\text{–}X_2} \quad \Rightarrow \quad L = \frac{\xi(L\text{–}X_2)}{X_2}$$

$$\begin{aligned} A_T &= L + L\text{–}X_2 + L\text{–}X \\ &= \tfrac{\xi(L\text{–}X_2)}{X_2} + L\text{–}X_2 + + L\text{–}X \\ &= (L\text{–}X_2)\left(1 + \tfrac{\xi}{X_2}\right) + L\text{–}X \end{aligned}$$

$$(L\text{–}X_2) = \frac{A_T - (L\text{–}X)}{\left(1 + \frac{\xi}{X_2}\right)}$$

$$\begin{aligned} \tfrac{dX}{dt} = \tfrac{d(L\text{–}X)}{dt} &= k_c(L\text{–}X_2) \\ &= \tfrac{k_c}{\left(1+\frac{\xi}{X_2}\right)}(A_T - (L\text{–}X)) \\ &= k_{obs}(A_T - (L\text{–}X)) \end{aligned}$$

$$\int \frac{d(L\text{–}X)}{A_T - (L\text{–}X)} = \int k_{obs}dt$$

$$-\ln[A_T - (L\text{–}X)] = k_{obs}t + B$$

$$@t = 0, L\text{–}X = 0 \Rightarrow B = -\ln A_T$$

$$\ln[A_T - (L\text{–}X)] - \ln A_T = -k_{obs}t$$

$$\ln\left(\frac{A_T - (L\text{–}X)}{L_T}\right) = -k_{obs}t$$

$$e^{-k_{obs}t} = \frac{A_T - (L\text{–}X)}{A_T}$$

$$L\text{–}X(t) = X(t) = A_T\left(1 + e^{-k_{obs}t}\right) \qquad \text{(eq. 1)}$$

$$k_{obs} = \frac{k_c}{\left(1 + \frac{\xi}{X_2}\right)} = \frac{k_c(X_2)}{X_2 + \xi} \qquad \text{(eq. 4)}$$

Appendix II

Kinetic Equations for the Alkylation of hRXRα LBD Cysteine Residues by DTNB

Kinetic Equations for the Alkylation of hRXRα LBD Cysteine Residues by DTNB

$$\begin{array}{ccccc} C + X_2 & \overset{K}{\rightleftharpoons} & O + X_2 & & \\ \xi \downarrow\uparrow & & \downarrow\uparrow \xi & & \\ C\text{–}X_2 & \underset{K}{\rightleftharpoons} & O\text{–}X_2 & \overset{k_f}{\rightarrow} & O\text{–}X + X \end{array} \qquad \text{(eq. 7)}$$

$X_2 = \text{DTNB}$, $X = \text{TNB}$

$C = \text{RXR in closed conformation}$

$O = \text{RXR in open conformation}$

$P_T = \text{Total amount of protein and derivatives}$

$X_2 \gg P_T$

$$K = \frac{O}{C} = \frac{O\text{–}X_2}{C\text{–}X_2} \quad \Rightarrow \quad C\text{–}X_2 = \frac{O\text{–}X_2}{K}$$

$$\xi = \frac{(O)(X_2)}{O\text{–}X_2} = \frac{(C)(X_2)}{C\text{–}X_2} \quad \Rightarrow \quad C = \frac{\xi\,(C\text{–}X_2)}{X_2} = \frac{\xi}{X_2}\left(\frac{O\text{–}X_2}{K}\right)$$

$$
\begin{aligned}
P_T &= C + O + O\text{–}X_2 + C\text{–}X_2 + O\text{–}X \\
&= \left(\tfrac{\xi}{X_2}\right)\left(\tfrac{O\text{–}X_2}{K}\right) + \tfrac{\xi(O\text{–}X_2)}{X_2} + O\text{–}X_2 + \tfrac{O\text{–}X_2}{K} + O\text{–}X \\
&= (O\text{–}X_2)\left\{\tfrac{\xi}{K(X_2)} + \tfrac{\xi}{X_2} + 1 + \tfrac{1}{K}\right\} + O\text{–}X \\
&= (O\text{–}X_2)\left\{\tfrac{\xi}{X_2}\left(1 + \tfrac{1}{K}\right) + 1 + \tfrac{1}{K}\right\} + O\text{–}X \\
&= (O\text{–}X_2)\left(1 + \tfrac{1}{K}\right)\left(1 + \tfrac{\xi}{X_2}\right) + O\text{–}X
\end{aligned}
$$

$$
(O\text{–}X_2) = \frac{P_T - (O\text{–}X)}{\left(1 + \frac{1}{K}\right)\left(1 + \frac{\xi}{X_2}\right)}
$$

$$
\begin{aligned}
\tfrac{dX}{dt} = \tfrac{d(O\text{–}X)}{dt} &= k_f(O\text{–}X_2) \\
&= \frac{k_f}{\left(1+\frac{1}{K}\right)\left(1+\frac{\xi}{X_2}\right)}(P_T - (O\text{–}X)) \\
&= \left(\tfrac{k_f K}{K+1}\right)\left(\tfrac{X_2}{\xi+X_2}\right)(P_T - (O\text{–}X)) = k_{obs}(P_T - (O\text{–}X))
\end{aligned}
$$

$$
\int \frac{d(O\text{–}X)}{P_T - (O\text{–}X)} = \int k_{obs}dt
$$

$$
-\ln[P_T - (O\text{–}X)] = k_{obs}t + B
$$

$$
@t = 0, O\text{–}X = 0 \Rightarrow B = -\ln P_T
$$

$$
\ln[P_T - (O\text{–}X)] - \ln P_T = -k_{obs}t
$$

$$
\ln\left(\frac{P_T - (O\text{–}X)}{P_T}\right) = -k_{obs}t
$$

$$
e^{-k_{obs}t} = \frac{P_T - (O\text{–}X)}{P_T}
$$

$$
O\text{–}X(t) = X(t) = P_T\left(1 + e^{-k_{obs}t}\right) \qquad \text{(eq. 1)}
$$

$$k'_f = \lim_{X_2 \to \infty} k_{obs} = \lim_{X_2 \to \infty} \left(\frac{k_f K}{K+1} \right) \left(\frac{X_2}{\xi + X_2} \right) = \left(\frac{k_f K}{K+1} \right) \qquad \text{(eq. 9)}$$

$$-RT \ln K = \Delta G^\circ = \Delta G^\circ(\mathrm{H_2O}) - m[\mathrm{GuHCl}] \qquad \text{(eq. 10)}$$

$$K = e^{\left(\frac{\Delta G^\circ(\mathrm{H_2O}) - m[\mathrm{GuHCl}]}{RT}\right)} \qquad \text{(eq. 11)}$$